Culebras, M.; Serrano-Claumarchirant, JF.; Sanchis Sánchez, MJ.; Landfester, K.; Cantarero, A.; Gomez- Clari, CM.; Muñoz-Espí, R. (2018). Conducting PEDOT Nanoparticles: Controlling Colloidal Stability
and Electrical Properties. The Journal of Physical Chemistry C. 122(33):19197-19203. https://doi.org/10.1021/acs.jpcc.8b04981

Conducting PEDOT Nanoparticles: Controlling Colloidal Stability and Electrical Properties

Mario Culebras,[†,‡] José F. Serrano-Claumarchirant,[†] Maria J. Sanchis,[¶] Katharina Landfester,[§] Andrés Cantarero,[‖] Clara M. Gómez,[†] and Rafael Muñoz-Espí[*,†]

†*Institute of Materials Science (ICMUV), Universitat de València, c/ Catedràtic José Beltrán 2, 46980 Paterna, Spain*

‡*Stokes Laboratories, Bernal Institute, University of Limerick, Ireland*

¶*Department of Applied Thermodynamics, ETSII, Institute of Electric Technology, Universitat Politècnica de València, 46022 València, Spain.*

§*Max Planck Institute for Polymer Research, Ackermannweg 10, Mainz 55128, Germany*

‖*Institute for Molecular Sciences (ICMol), Universitat de València, c/ Catedràtic José Beltrán 2, 46980 Paterna, Spain*

E-mail: rafael.munoz@uv.es

Phone: +34-963544210

Abstract

The synthesis of conducting polymer nanoparticles by oxidative polymerization can be a challenge, because the addition of oxidizers may compromise the colloidal stability of the system. In this work, we report the successful synthesis poly(3,4-ethylenedioxythiophene) (PEDOT) nanoparticles by means of miniemulsion polymerization. We study the role of oxidizing agents (iron(III) *p*-toluenesulfonate and hydrogen peroxide) during the particle formation particles and in the electric properties. The presence hydrogen peroxide is demonstrated to be crucial in the macroscopic stability of the suspensions and the morphology of the resulting nanoparticles. The obtained suspensions, containing particles of diameters of around 30 nm, are stable for several months. The electrical conductivity increases with increasing the content of iron(III) *p*-toluenesulfonate, but it decreases with addition of hydrogen peroxide, which can be explained by secondary reactions in the polymerization process.

Introduction

Organic electronics has been attracting an increasing attention of the energy-materials community over the last decade. In particular, conducting polymers have become the focus of many investigations due to their better processing and, sometimes, even better performance for electronic applications than other materials, which make them especially promising in the scientific race towards more sustainable energy production.[1,2] The main advantages of conducting polymers are the low cost of the raw materials, their flexibility, their easy chemical modification, the non-toxicity, and their versatility in a wide range of applications.[3–5] It is therefore not surprising that they are being used in different energy-related devices, including organic solar cells,[6,7] supercapacitors,[8–11] and thermoelectric devices.[12,13]

The transport of current between polymer chains is possible because of the existence of conjugated π-bonds along the polymer backbone. Electrons from the π-bonds are able to move, generating free charges along the polymer chains, with a doping effect in the fi-

nal material.[13–15] The control of the doping level in organic semiconductors is crucial for a good performance. For instance, the maximum thermoelectric efficiency in conducting polymers is reached at an optimum doping level. At this point, the best compromise between the electrical conductivity and the Seebeck coefficient is obtained. The doping level can be controlled in different manners: with chemical reductants, such as hydrazine[14] or tetrakis(dimethylamino)ethylene (TDEA),[16] and by electrochemical (de)doping.[15] Nanostructuration of conducting polymers can be a powerful tool to increase their performance for energy applications. As an example, the use of nanostructurated electrodes of conducting polymers in supercapacitors increases the surface area, thus increasing the capacitance of the final device.[10,17,18] In the case of thermoelectric polymers, the thermal conductivity can be tailored through nanowire structuration due to phonon scattering.[19]

Currently, there are two kinds of methods to fabricate nanostructurated materials: top-down and bottom-up methods.[20–23] Top-down methods are based on the reduction of components and structures from the highest to the lowest size. This type of nanotechnology, including techniques such as optical lithography and electron-beam lithography,[24] is the most developed until now. Bottom-up techniques consist on the *in situ* building of nanostructures from the lowest to the highest size, as it is the case, for example, for the polymerization facilitated by templates. Depending on the nature of the template employed during the synthesis, there are two kinds of methods: hard-template and soft-template methods. Hard-template strategies are based on the use of a rigid template, such as alumina or polycarbonate membranes,[4] while nanostructuring by soft-template methods is mostly attained by the presence of surfactants or other organic structure-directing agents.[25–27]

Soft-template methods, especially those based on the miniemulsion technique, have been employed to synthesize stable polymer particle suspensions of a wide range of materials, including polystyrene, poly(mehtyl methacrylate) (PMMA) or polyurethane.[28] The miniemulsion technique allows for a variety of functionalities on the surface of the polymer nanoparticles by using functional comonomers during the synthesis.[29,30] The resulting suspensions

can be used for the preparation of coatings for specific applications, such as electrodes in supercapacitors[31] or solar cells.[32]

Only very few works have focused so far on the preparation of conducting polymer nanoparticles from poly(3,4 ethylenedioxythiophene) (PEDOT),[26,27] and they have involved the use of large amounts of surfactants and the addition of insulating polymer additives as stabilizers,[33] which is disadvantageous for the electrical properties. Moreover, the control of the doping level of the conducting polymer is not very efficient, because the addition of an oxidizing agent destabilizes the emulsion, which results in bulk polymerization.

In this work, we report the synthesis of stable PEDOT nanoparticles with a well-defined spherical morphology (size around 35 nm). The suspensions, macroscopically stable for several months, are used for the preparation of films with defined electrical properties.

Experimental Section

Materials

3,4-ethylenedioxythiophene (EDOT, 97%, Sigma Aldrich), iron(III) *p*-toluenesulfonate hexahydrate (FeTos, 98%, Sigma Aldrich), hydrogen peroxide (30% in H_2O PanReac AppliChem), and Lutensol AT 50 (BASF SE, a non-ionic surfactant based on ethylene oxide that follows the formula R–O(CH_2CH_2O)$_{50}$H where R is linear, saturated $C_{16}C_{18}$ fatty alcohol) were used as received.

Synthesis of PEDOT Nanoparticles

The synthesis of PEDOT nanoparticles was carried out by miniemulsion polymerization.[26,27] Lutensol AT 50 (0.05 g, 2.0×10^{-5} mol) was dissolved in 40 mL of ultra-pure water. EDOT (0.2 mL, 1.8×10^{-3} mol) was added to this solution, and the mixture was pre-emulsified by magnetic stirring for 10 min and ultrasonified afterwards by using a a Branson 450-D sonifier (1/2-inch tip, 70% amplitude in a pulsed mode, 0.9 s pulse, 0.1 s pause, 5 min).

The obtained white dispersion was transferred to a reaction flask and placed in an oil bath thermostatted at 45 °C under magnetic stirring. Immediately afterwards, 25 mL of a FeTos aqueous solution (see Table 1) was added to the reaction flask. The mixture was left to polymerize for 24 h.

The purification of PEDOT nanoparticles was carried out by centrifugation at 13,000 rpm during 20 min, washing always with water. The process was repeated until observing a transparent color in the supernatant solution, indicating that all the excess of FeTos had been completely removed.

The purified nanoparticles were redispersed in 40 mL of ultra-pure water by sonicating for 30 min in a sonication bath, for 20 min under the ultrasonication tip (same conditions as above), and again for 20 min in the sonication bath.

The different experimental conditions used in the work are listed in Tables 1 (study of the EDOT:FeTos molar ratio) and 2 (study of the H_2O_2 concentration). The addition of H_2O_2 was carried out 1 h after finishing the addition of FeTos solution.

Table 1: Amounts of the reactants for samples prepared with different EDOT:FeTos molar ratio.

	EDOT:FeTos molar ratio			
Reactant	**(1:0.5)**	**(1:1)**	**(1:2)**	**(1:3.5)**
Lutensol AT 50 (g)	0.05	0.05	0.05	0.05
EDOT (mL)	0.2	0.2	0.2	0.2
FeTos (M)	1.4×10^{-2}	2.8×10^{-2}	5.7×10^{-2}	1.0×10^{-1}

Table 2: Amounts of the reactants for samples prepared with different concentrations of H_2O_2 while keeping constant the EDOT:FeTos (molar ratio 1:1).

	H_2O_2 concentration (M)				
Reactant	**0**	**7.5×10^{-3}**	**1.5×10^{-2}**	**3.7×10^{-2}**	**7.5×10^{-2}**
Lutensol AT 50 (g)	0.05	0.05	0.05	0.05	0.05
EDOT (mL)	0.2	0.2	0.2	0.2	0.2
FeTos (M)	2.8×10^{-2}	2.8×10^{-2}	2.8×10^{-2}	2.8×10^{-2}	2.8×10^{-2}
H_2O_2 (mL)	0.0	0.05	0.10	0.25	0.50

Formation of Films and Pellets

PEDOT nanoparticle films were obtained by solvent-casting method in a glass substrate at 60 °C under vacuum. PEDOT:FeTos pellets were obtained by drying the dispersion at 60 °C under vacuum and compacting the resulting powder in a pellet die (1/2 in of diameter) under pressure.

Characterization Techniques

Transmission electron microscopy (TEM) was carried out in a JEOL JEM-1010 microscope operated at 100 kV and coupled with a digital camera MegaView III. The particle size was analyzed from the TEM images using the software Image J.[34]

The electrical conductivity of the films was determined with a home-made equipment by using the van der Pauw method, in which four contacts are used to eliminate the effect of the contact resistance,[35]

$$e^{-\pi d R_1 \sigma} + e^{-\pi d R_2 \sigma} = 1 \tag{1}$$

where d is the sample thickness previously measured, R_1 and R_2 are the electrical resistance of the films. A Keithley 2400 was used as a driving source. For the case of pellets, the electrical conductivity measurements were carried out by using broadband dielectric relaxation spectroscopy in a Novocontrol Broadband Dielectric spectrometer (Hundsagen, Germany).

Seebeck effect measurements were conducted in a home-made experimental setup consisting of two copper blocks, one heated by an electrical resistance and the other cooled by a water flow. The sample is placed in between these two blocks. A temperature difference is created across the sample and the resulting voltage is recorded. The Seebeck coefficient can be determined as the ratio between the electrical potential, ΔV, and the temperature difference, ΔT, that is,

$$S = \frac{\Delta V}{\Delta T} \tag{2}$$

The temperature was controlled with a Lakeshore 340 temperature controller and two PT100 resistors previously calibrated. To record the potential, a Keithley 2750 multimeter switching system was employed. Both instruments were coupled by using a self-written LabView software.

The film thickness was measured with the aid of a profilometer (Optical Profilometer Dektak 150). Reported values are an average of at least 5 different measurements per film.

Raman scattering measurements were carried out at room temperature in backscattering configuration by using a Jobin Yvon T64000 spectrometer equipped with a liquid-nitrogen cooled open electrode charge-coupled device (OECCD camera). The excitation line of 514.53 nm was provided by an Ar/Kr laser focused onto the sample using a 100× microscope objective with a numerical aperture $NA = 0.90$ (Olympus). This setup focuses the light on an area around 1μm on top of the sample. Special care was taken to avoid sample heating during the experiments, limiting the power down to a few μW.

Fourier transform infrared spectroscopy (FTIR) measurements were performed in a Nicolet Nexus FTIR spectrometer over the range from 450 to 4000 cm^{-1} with the attenuated total reflectance (ATR) accessory by co-addition of 60 scans with a spectral resolution of 2 cm^{-1}.

UV-Vis spectroscopy measurements were carried out in a Shimadzu UV-2501PC spectrophotometer covering the range from 1100 to 300 nm. Quartz cells were employed.

Results and Discussion

PEDOT nanoparticles were synthesized by using oxidative miniemulsion polymerization. White miniemulsions were obtained after emulsification of the monomer (EDOT) in a continuous aqueous phase containing Lutensol AT 50 as a non-ionic surfactant. In a first set of

experiments, *p*-toluenesulfonate hexahydrate (FeTos) was used as a single oxidant, varying its proportion with respect to the monomer (*cf.* Table 1). In a second set (*cf.* Table 2), the EDOT/FeTos ratio was kept constant as 1:1 and H_2O_2 was subsequently added after FeTos, which led to clearly more stable particle dispersions, as discussed in the following. In all cases, immediately after the addition of FeTos, the dispersions turned to a dark blue color, characteristic for PEDOT dispersions and solutions.

In the absence of H_2O_2, dynamic light scattering (DLS) measurements of the PEDOT suspensions obtained after polymerization indicated sizes above 1 μm, so that they are too large to be taken as reliable. Transmission electron microscopy (TEM) micrographs, presented in Figure 3, show that the formed particles are clearly smaller than the values obtained by DLS, which can be correlated with the formation of aggregates that tend to sediment during the measurement. Indeed, sedimentation in these dispersions can be macroscopically observed already after a few days, or even hours in some cases (see photographs in Supporting Information, Figure S1). At the highest EDOT:FeTos molar ratio used, the loss of a defined particle morphology and the formation of aggregates is also evident from TEM images (Figure 3(d)). At the initial step of the miniemulsion process, the EDOT droplets can be assumed to be spherical because the monomer is a liquid, which is dispersed in water. When the oxidant (FeTos) is added, the iron(III) ions migrate to the EDOT–water interface and oxidize the monomer (EDOT) to form the polymer (PEDOT). Iron(III) ions are thereby reduced to iron(II). EDOT is only sparingly soluble in water. However, when the FeTos content is very high, homogeneous nucleation outside the droplets is likely to occur and may lead to the flake-like aggregates observed.

For the following experiments, H_2O_2 was added after FeTos to give overall concentrations in the continuous phase from 7.5×10^{-3} to 7.5×10^{-2} M. The molar ratio EDOT:FeTos was kept at 1:1, because it was shown to be optimum in terms of macroscopic colloidal stability and particle morphology. The corresponding TEM images are shown in Figure 2 (see also SEM images in Supporting Information, Figure S2). DLS measurements of these samples

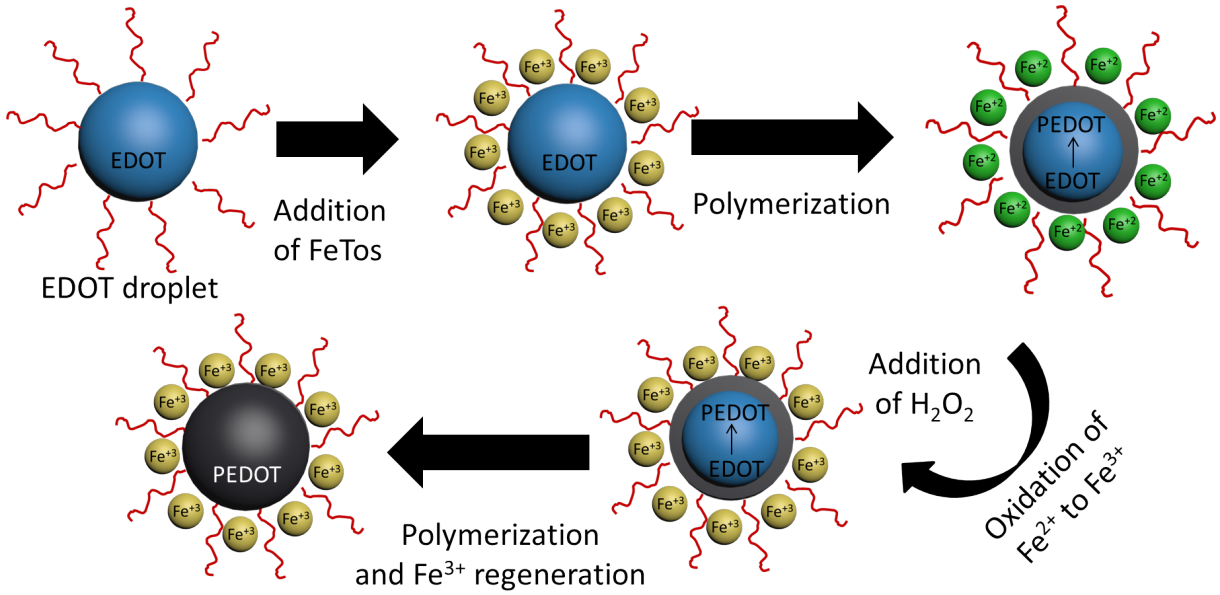

Figure 1: Scheme representation of the formation of PEDOT nanoparticles in the presence of FeTos and H_2O_2.

indicated sizes in all cases in the range 90–150 nm, with deviations from the mean size of around ±30%. Intensity and number distribution provide similar values. In contrast, the sizes observed in TEM micrographs (*cf.* size distributions in Figure 2(e)) are of 30–40 nm, significantly smaller than the values obtained by DLS. This difference between TEM and DLS results can be explained by the formation aggregates of a few particles with defined size. However, it is very important to mention that the suspensions prepared in the presence of H_2O_2 remained stable after several months. Even if aggregates form, as indicated by DLS, they are small, of defined size, and stable over time, without macroscopic signs of coalescence or Ostwald ripening (Supporting Information, Figure S1).

The results indicate clearly that the addition of H_2O_2 leads to particles with better defined morphology, more homogeneous size distribution, and very stable dispersions thereof. At the time of addition of H_2O_2, 1 h after FeTos addition, the polymerization of EDOT is in progress, but a substantial amount of polymer is already present at the interface, where Fe^{2+} ions (resulting from the reduction of Fe^{3+} to Fe^{2+} during the oxidative polymerization) are also present. When H_2O_2 is added, Fe^{2+} is oxidized back to Fe^{3+}, so that the polymerization

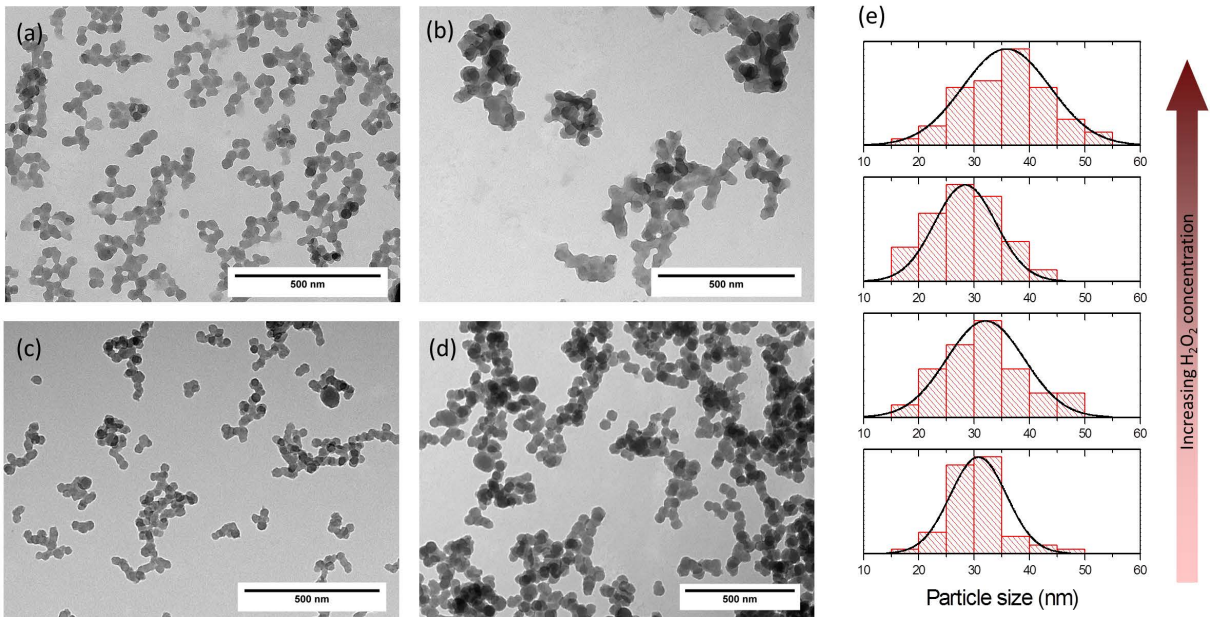

Figure 2: TEM images of PEDOT nanoparticles with H_2O_2: (a) 7.5 $\cdot 10^{-3}$ M, (b) 1.5 $\times 10^{-2}$ M, (c) 3.7 $\times 10^{-2}$ M, (d) 7.5 $\times 10^{-2}$ M. (e) Particle size distribution.

of EDOT can further take place. Particles of relatively homogeneous size and shape are formed, so that stable suspensions are obtained. A schematic representation of the formation of PEDOT particles in the presence of FeTos and H_2O_2 is depicted in Figure 1.

Electrical conductivity and the Seebeck coefficient, both parameters related to the doping level, were measured for films prepared by drop-casting from dialyzed dispersions of the PEDOT nanoparticles. Glass substrates were coated with the PEDOT suspension and the solvent (water) was evaporated at 60 °C under vacuum. The thickness of the prepared films was in the range 0.5–1 μm. The electrical conductivity was measured by using the van der Pauw method, as described in the experimental section. Figure 4 shows the electrical conductivity and the Seebeck coefficient of the PEDOT nanoparticles as a function of the FeTos concentration. The electrical conductivity increases from 2.1×10^{-6} to 2.6 S/cm when the FeTos concentration increases from 0.014 to 0.1 M. The increase in the concentration of FeTos during the synthesis results in a more pronounced oxidation in the PEDOT chains, producing a doping process in the PEDOT nanoparticles.[14,15] The Seebeck coefficient at 0.014 M could not be measured because of the high electrical resistance of the sample, which

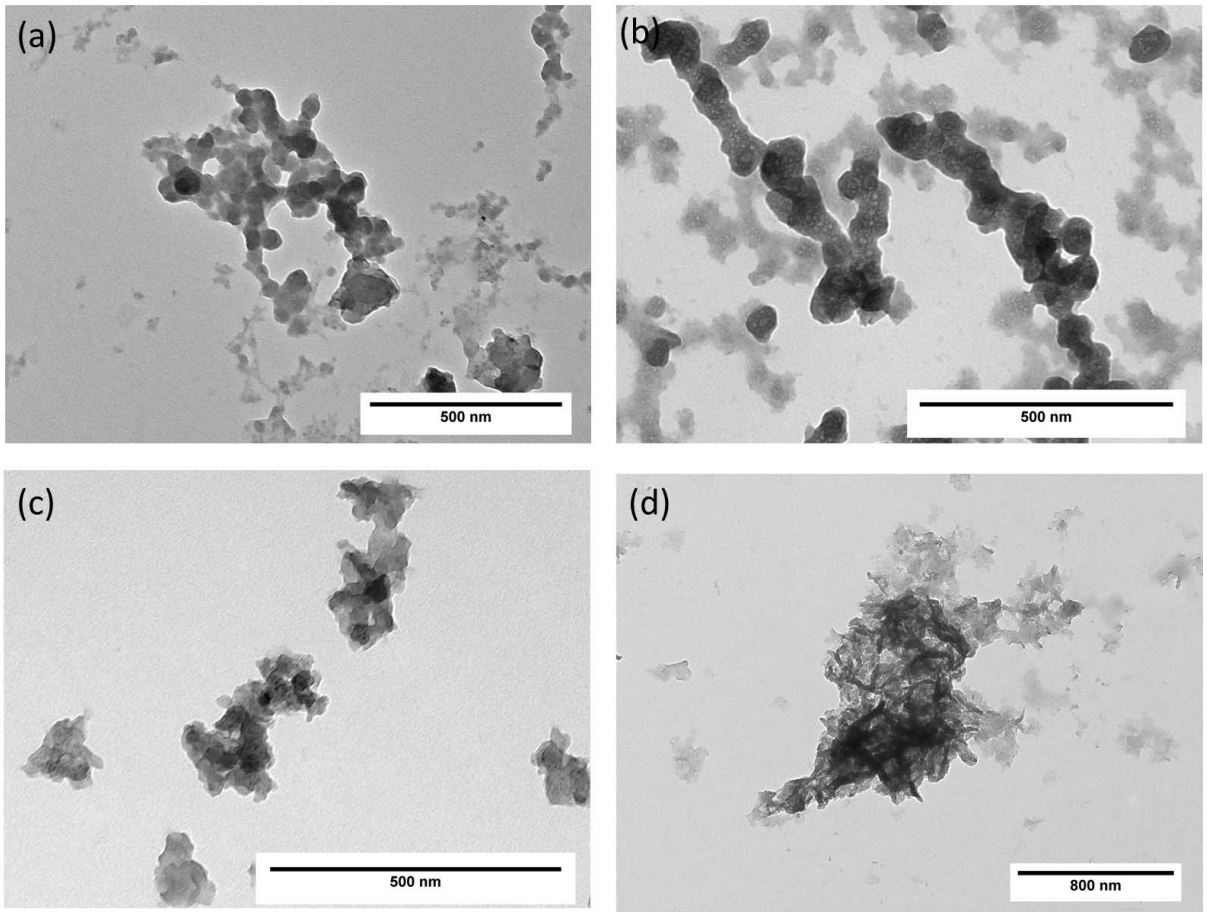

Figure 3: TEM images of PEDOT nanoparticles prepared with different EDOT:FeTos molar ratios: (a) 1:0.5, (b) 1:1, (c) 1:2, (d) 1:3.5.

originate a large noise in the signal. In contrast, the measurements for samples prepared at higher concentration of FeTos yielded very clean signals, corresponding to a Seebeck coefficient of around 30–35 μV/K for particles synthesized with a FeTos concentration between 0.028 and 0.057 M. These values correspond to low-doped PEDOT. At even higher concentration of FeTos (0.1 M), the Seebeck coefficient was around 12.6 μV/K. This value is very similar to highly doped PEDOT films.[14,15]

To study the doping degree, the samples were analyzed by Raman and UV-Vis spectroscopy. Figure 5(a) shows the Raman spectra of PEDOT nanoparticles prepared with different concentrations of FeTos. No Raman signal has been observed at low FeTos concentration (molar ratio EDOT:FeTos 1:0.5), which indicates a low polymerization degree. The

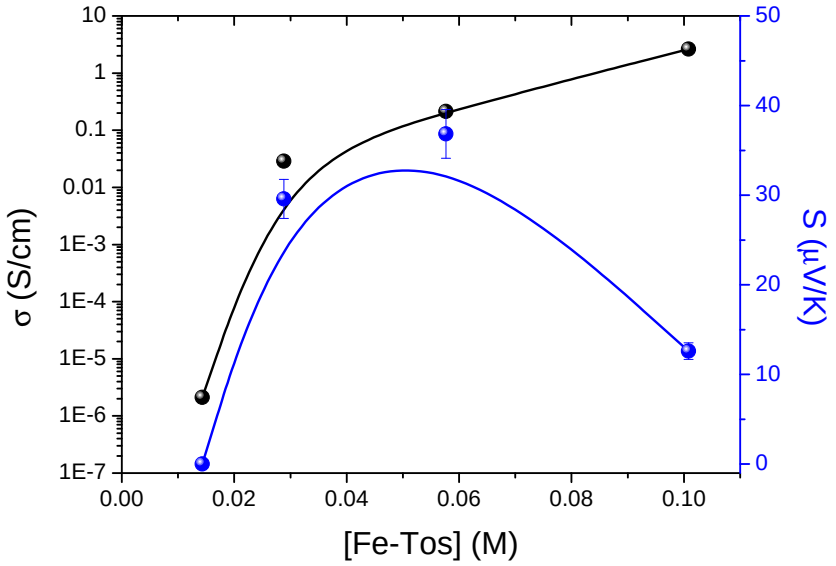

Figure 4: Electrical conductivity, and Seebeck coefficient of PEDOT nanoparticles as a function of FeTos concentration.

Raman intensity is maximum at a molar ratio EDOT:FeTos of 1:1, indicating a low doping level in PEDOT. The Raman signal is high when the number of neutral π-bonds increases in the polymer backbone.[36,37] However, the Raman signal decreases at even higher content of FeTos because the final material presents a higher doping level.

The same trend was observed in the UV-Vis results, shown in Figure 5(b). The spectrum of the sample prepared at EDOT:FeTos molar ratio 1:0.5 is different from the spectra at higher molar ratios. The absorption is likely to be caused by olygomeric species of EDOT, which would explain the low electrical conductivity. However, spectra for PEDOT nanoparticles prepared at molar ratios higher than 1:0.5 present the typical curve shape for PEDOT. The absorption related with the polaronic and bipolaronic states (800–1000 nm)[38] increases at higher concentration of FeTos, while the absorption responsible for the neutral π-bonds increases at lower concentration.[38]

For the case of the nanoparticles prepared with H_2O_2, the electrical conductivity was determined in both film and pellet conformations. The electrical conductivity was obtained with the van der Paw method for the case of film, while for the case of pellet the values

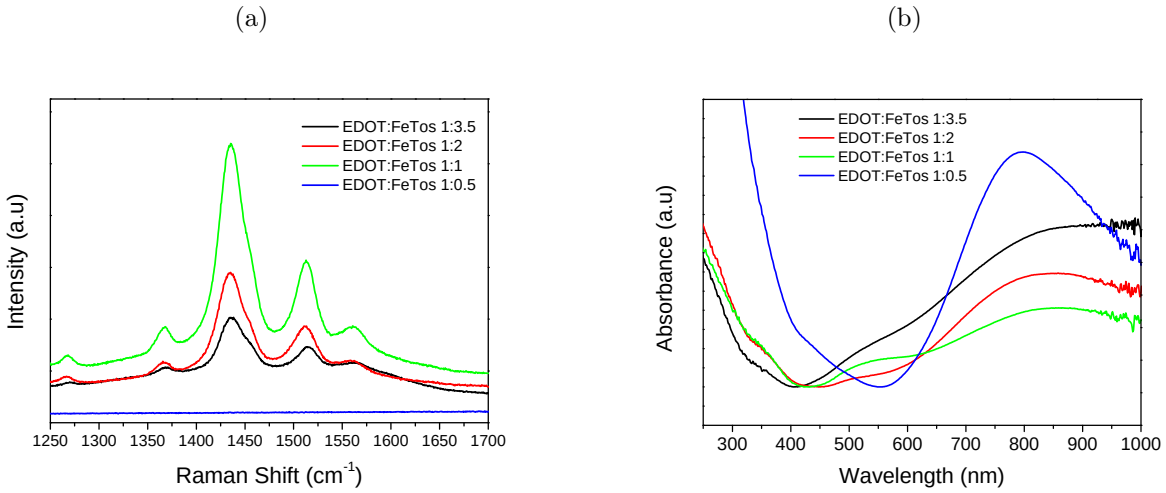

Figure 5: (a) Raman and (b) UV-Vis spectra of PEDOT at different EDOT:FeTos molar ratios.

were obtained using broadband dielectric spectroscopy. Figure 6(a) shows the electrical

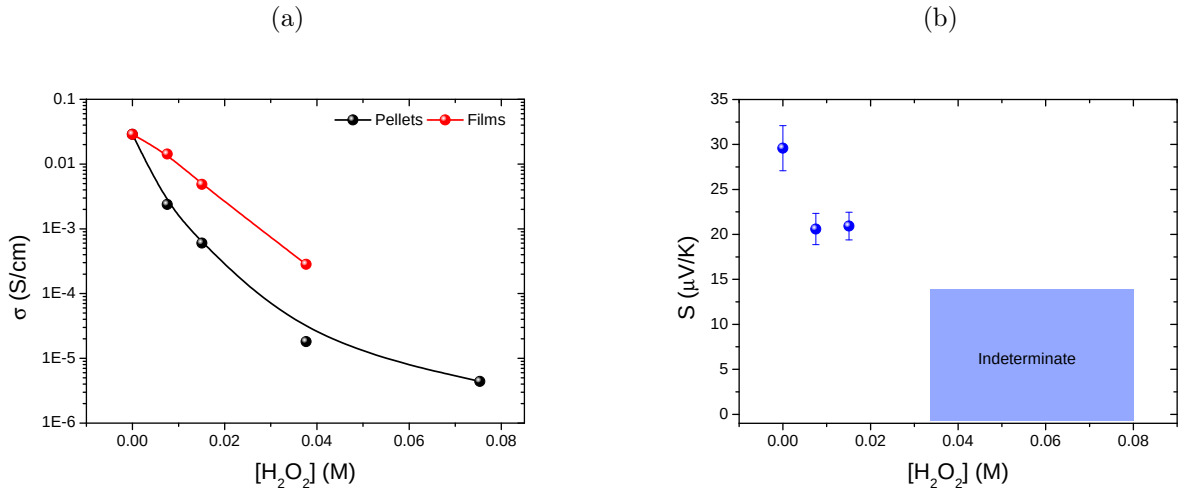

Figure 6: (a) Electrical conductivity and (b) Seebeck coefficient of PEDOT as a function of H_2O_2 concentration.

conductivity for both, pellets and films, as a function of the H_2O_2 concentration employed during the synthesis. The electrical conductivity decreases in both cases with increasing H_2O_2 concentration. However, the values of the electrical conductivity were higher in films when compared to the pellets due to the large number of defects and interfaces in pellets. This fact produces more difficulties for the electric transport across the pellet compared

to the thin film. The decrease of the electrical conductivity can be generated by molecular changes on the PEDOT structure. The values of the Seebeck coefficient are plotted in Figure 6(b). At higher H_2O_2 concentrations, the Seebeck coefficient could not be measured due to the insulating nature of the PEDOT nanoparticles. At low concentration, the Seebeck values were lower than the particles obtained without H_2O_2. This trend is not unusual, because the electrical conductivity and the Seebeck coefficient decreases simultaneously. Thus, the results indicate that H_2O_2 is not producing a de-doping process, but some changes into the molecular structure of PEDOT that generates a depletion of the electrical conductivity.

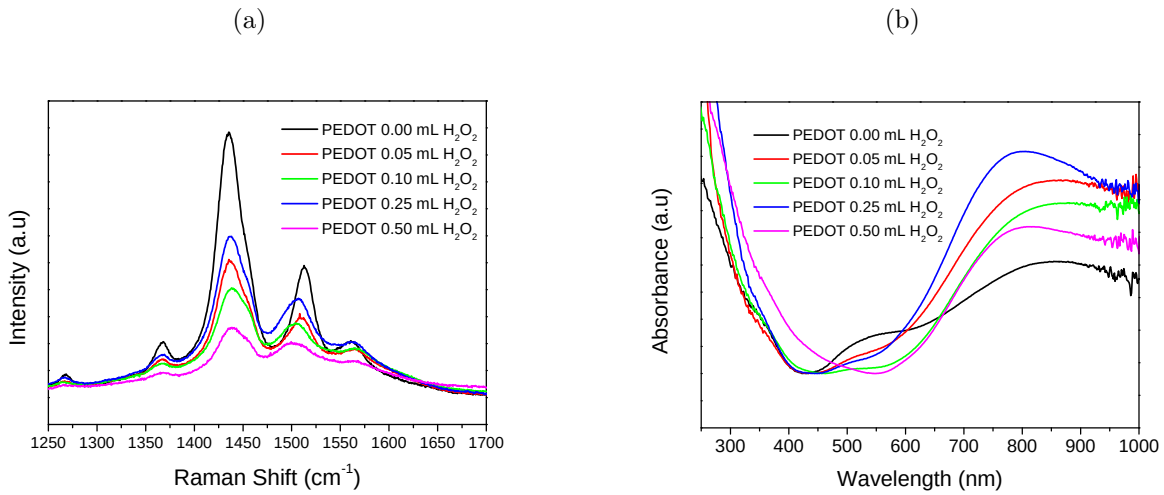

Figure 7: (a) Raman and (b) UV-Vis spectra of PEDOT at different H_2O_2 content H_2O_2.

Figure 7(a) shows the Raman spectra of PEDOT nanoparticles at different H_2O_2 volumes added during the synthesis. The spectra present the typical vibrational modes for PEDOT in the region between 1250 and 1700 cm^{-1}. The intensity of the Raman signal decreases with the presence of H_2O_2, which corresponds to a decrease of the number of neutral π-bonds along the polymer backbone. Also a shift of the signal related with the asymmetric C=C stretching is observed. This fact is also an indication of the decrease in the electrical conductivity, given by some changes in the conjugation of the PEDOT chains. Figure 7(b) shows the UV-Vis spectra of PEDOT nanoparticles at different H_2O_2 volumes added during the synthesis. The absorption of the oxidized states is observed in all cases, which indicates a high oxidation

in the polymer chains. However, the absorption related to the conjugated neutral π-bond is very low and decreases with the addition of H_2O_2. A possible explanation for this trend is that, during the polymerization process, the radicals generated in the conjugated neutral π-system can interact with the $\cdot$OH radicals from the H_2O_2. The hydroxyl radicals are bonded to the polymer backbone breaking the conjugation of the PEDOT chain. The break of the conjugation produces a big decrease in the electrical conductivity, because charges cannot propagate along the polymer chains. Accordingly, the electrical conductivity decreases five orders of magnitude with the addition of 0.5 mL of H_2O_2. The presence of hydroxyl groups in the polymer backbone was evidenced by FTIR analysis (Supporting Information, Figure S3).

Conclusions

PEDOT nanoparticles have been synthesized by using oxidative miniemulsion polymerization. The electrical conductivity increases with the contraction of *p*-toluenesulfonate hexahydrate, used as an oxidizer. A homogeneous spherical morphology is only obtained in the presence of H_2O_2 during the synthesis, which also allows for suspensions that are macroscopically stable for several months. However, the electrical conductivity of the nanoparticles decreases with the concentration of H_2O_2 due to secondary reactions between the hydroxide radicals and the PEDOT chains. The results indicate that it is possible to reach PEDOT nanoparticles dispersions with conductivity values from 1 to 10^{-6} S/cm.

Associated Content

Supporting Information

Photographs showing macroscopic stability of suspensions prepared with and without H_2O_2, SEM images, and FTIR spectra.

Acknowledgments

The authors acknowledge the financial support from the Dirección General de Investigación Científica y Técnica through a grant of the Program Consolider Ingenio (grant no. CSD2010-0044) and the grant no. MAT2016-63955-R. The authors also thank the Max Planck Society through the funding of the Max Planck Partner Group on Colloidal Methods for Multifunctional Materials (CM3) at the University of Valencia, headed by RME. MC acknowledges the financial support by the Spanish Ministry of Education, Culture and Sport through the FPU training program and the German Academic Exchange Service (DAAD) for a short-term research scholarship at the Max Planck Institute for Polymer Research. Finally, RME thanks the financial support from the Spanish Ministry of Economy and Competitiveness through a Ramón y Cajal grant (grant no. RYC-2013-13451).

References

(1) Connolly, D.; Lund, H.; Mathiesen, B. V.; Leahy, M. A review of computer tools for analysing the integration of renewable energy into various energy systems. *Appl. Energy* **2010**, *87*, 1059–1082.

(2) Lund, H.; Mathiesen, B. V. Energy system analysis of 100% renewable energy systems—The case of Denmark in years 2030 and 2050. *Energy* **2009**, *34*, 524–531.

(3) Shakouri, A. In *Ann. Rev. Mater. Res.*; Clarke, DR and Fratzl, P„ Ed.; Annual Review of Materials Research; 2011; Vol. 41; pp 399–431.

(4) Mijangos, C.; Hernandez, R.; Martin, J. A review on the progress of polymer nanostructures with modulated morphologies and properties, using nanoporous AAO templates. *Prog. Polym. Sci.* **2016**, *54-55*, 148–182.

(5) Kango, S.; Kalia, S.; Celli, A.; Njuguna, J.; Habibi, Y.; Kumar, R. Surface modifica-

tion of inorganic nanoparticles for development of organic-inorganic nanocomposites-A review. *Prog. Polym. Sci.* **2013**, *38*, 1232–1261.

(6) Guenes, S.; Neugebauer, H.; Sariciftci, N. S. Conjugated polymer-based organic solar cells. *Chem. Rev.* **2007**, *107*, 1324–1338.

(7) Sakurai, S.; Kawamata, Y.; Takahashi, M.; Kobayashi, K. Improved Photocurrent of a Poly (3,4-ethylenedioxythiophene)-ClO4-/TiO2 Thin Film-modified Counter Electrode for Dye-sensitized Solar Cells. *J. Oleo Sci.* **2011**, *60*, 639–646.

(8) Conway, B. E. *Electrochemical supercapacitors: scientific fundamentals and technological applications*; Springer Science & Business Media, 2013.

(9) Zhao, Z.; Richardson, G. F.; Meng, Q.; Zhu, S.; Kuan, H.-C.; Ma, J. PEDOT-based composites as electrode materials for supercapacitors. *Nanotechnology* **2016**, *27*, 042001.

(10) Wang, K.; Zhao, P.; Zhou, X.; Wu, H.; Wei, Z. Flexible supercapacitors based on cloth-supported electrodes of conducting polymer nanowire array/SWCNT composites. *J. Mater. Chem.* **2011**, *21*, 16373–16378.

(11) Guo, B.; Hu, Z.; An, Y.; An, N.; Jia, P.; Zhang, Y.; Yang, Y.; Li, Z. Nitrogen-doped heterostructure carbon functionalized by electroactive organic molecules for asymmetric supercapacitors with high energy density. *RSC Adv.* **2016**, *6*, 40602–40614.

(12) Ahiska, R.; Mamur, H. A review: Thermoelectric generators in renewable energy. *Int. J. Renew. Energy Res.* **2014**, *4*, 128–136.

(13) Culebras, M.; Gomez, C. M.; Cantarero, A. Review on Polymers for Thermoelectric Applications. *Materials* **2014**, *7*, 6701–6732.

(14) Culebras, M.; Cantarero, A.; Gómez, C. M. Enhanced thermoelectric performance of

PEDOT with different counter ions optimized by chemical reduction. *J. Mater. Chem. A* **2014**, *2*, 10109–10115.

(15) Culebras, M.; Uriol, B.; Gomez, C. M.; Cantarero, A. Controlling the thermoelectric properties of polymers: application to PEDOT and polypyrrole. *Phys. Chem. Chem. Phys.* **2015**, *17*, 15140–15145.

(16) Bubnova, O.; Khan, Z. U.; Malti, A.; Braun, S.; Fahlman, M.; Berggren, M.; Crispin, X. Optimization of the thermoelectric figure of merit in the conducting polymer poly(3,4-ethylenedioxythiophene). *Nat Mater* **2011**, *10*, 429–433.

(17) García-Barberá, A.; Culebras, M.; Roig-Sánchez, S.; Gómez, C. M.; Cantarero, A. Three dimensional PEDOT nanowires network. *Synth. Met.* **2016**, *220*, 208–212.

(18) Liu, R.; Duay, J.; Lee, S. B. Heterogeneous nanostructured electrode materials for electrochemical energy storage. *Chem. Commun.* **2011**, *47*, 1384–1404.

(19) Muñoz Rojo, M.; Martin, J.; Grauby, S.; Borca-Tasciuc, T.; Dilhaire, S.; Martin-Gonzalez, M. Decrease in thermal conductivity in polymeric P3HT nanowires by size-reduction induced by crystal orientation: new approaches towards thermal transport engineering of organic materials. *Nanoscale* **2014**, *6*, 7858–7865.

(20) Gregorczyk, K.; Knez, M. Hybrid nanomaterials through molecular and atomic layer deposition: Top down, bottom up, and in-between approaches to new materials. *Prog. Mater. Sci.* **2016**, *75*, 1–37.

(21) Hamley, I. Nanotechnology with soft materials. *Angew. Chem.-Int. Edit.* **2003**, *42*, 1692–1712.

(22) Cheng, J. Y.; Ross, C. A.; Smith, H. I.; Thomas, E. L. Templated self-assembly of block copolymers: Top-down helps bottom-up. *Adv. Mater.* **2006**, *18*, 2505–2521.

(23) Henzie, J.; Barton, J.; Stender, C.; Odom, T. Large-area nanoscale patterning: Chemistry meets fabrication. *Accounts Chem. Res.* **2006**, *39*, 249–257.

(24) Guo, L. J. Nanoimprint lithography: Methods and material requirements. *Adv. Mater.* **2007**, *19*, 495–513.

(25) Hood, M. A.; Mari, M.; Muñoz-Espí, R. Synthetic strategies in the preparation of polymer/inorganic hybrid nanoparticles. *Materials* **2014**, *7*, 4057–4087.

(26) Wu, C.-H.; Don, T.-M.; Chiu, W.-Y. Characterization and conversion determination of stable PEDOT latex nanoparticles synthesized by emulsion polymerization. *Polymer* **2011**, *52*, 1375–1384.

(27) Wu, C.-H.; Chiu, W.-Y.; Don, T.-M. Conductive composite particles synthesized via pickering emulsion polymerization using conductive latex of poly(3,4-ethylenedioxythiophene) (PEDOT) as stabilizer. *Polymer* **2012**, *53*, 1086–1092.

(28) Landfester, K. Miniemulsion Polymerization and the Structure of Polymer and Hybrid Nanoparticles. *Angew. Chem., Int. Ed. Engl.* **2009**, *48*, 4488–4507.

(29) Froimowicz, P.; Muñoz-Espí, R.; Landfester, K.; Musyanovych, A.; Crespy, D. Surface-Functionalized Particles: From their Design and Synthesis to Materials Science and Bio-Applications. *Curr. Org. Chem.* **2013**, *17*, 900–912.

(30) Crespy, D.; Landfester, K. Miniemulsion polymerization as a versatile tool for the synthesis of functionalized polymers. *Beilstein J. Org. Chem.* **2010**, *6*, 1132–1148.

(31) Tan, Y.; Zhang, Y.; Kong, L.; Kang, L.; Ran, F. Nano-Au@ PANI core-shell nanoparticles via in-situ polymerization as electrode for supercapacitor. *J. Alloy. Comp.* **2017**,

(32) Colberts, F. J.; Wienk, M. M.; Janssen, R. A. Aqueous Nanoparticle Polymer Solar Cells: Effects of Surfactant Concentration and Processing on Device Performance. *ACS Appl. Mater. Interfaces* **2017**, *9*, 13380–13389.

(33) Lv, L.-P.; Zhao, Y.; Vilbrandt, N.; Gallei, M.; Vimalanandan, A.; Rohwerder, M.; Landfester, K.; Crespy, D. Redox responsive release of hydrophobic self-healing agents from polyaniline capsules. *J. Am. Chem. Soc.* **2013**, *135*, 14198–14205.

(34) Schneider, C. A.; Rasband, W. S.; Eliceiri, K. W. NIH Image to ImageJ: 25 years of image analysis. *Nature methods* **2012**, *9*, 671–675.

(35) Van Der Pauw, L. J. A method of measuring the resistivityi and Hall coeficient on lamellae of arbitrary shape. *Philips Techinical Review* **1958**, *20*, 220–224.

(36) Garreau, S.; Louarn, G.; Buisson, J.; Froyer, G.; Lefrant, S. In situ spectroelectrochemical Raman studies of poly(3,4-ethylenedioxythiophene) (PEDT). *Macromolecules* **1999**, *32*, 6807–6812.

(37) Garreau, S.; Duvail, J.; Louarn, G. Spectroelectrochemical studies of poly(3,4-ethylenedioxythiophene) in aqueous medium. *Synth. Met* **2001**, *125*, 325–329.

(38) Chen, X.; Inganas, O. Three-step redox in polythiophenes: Evidence from electrochemistry at an ultramicroelectrode. *J. Phys. Chem.* **1996**, *100*, 15202–15206.

ToC Graphic

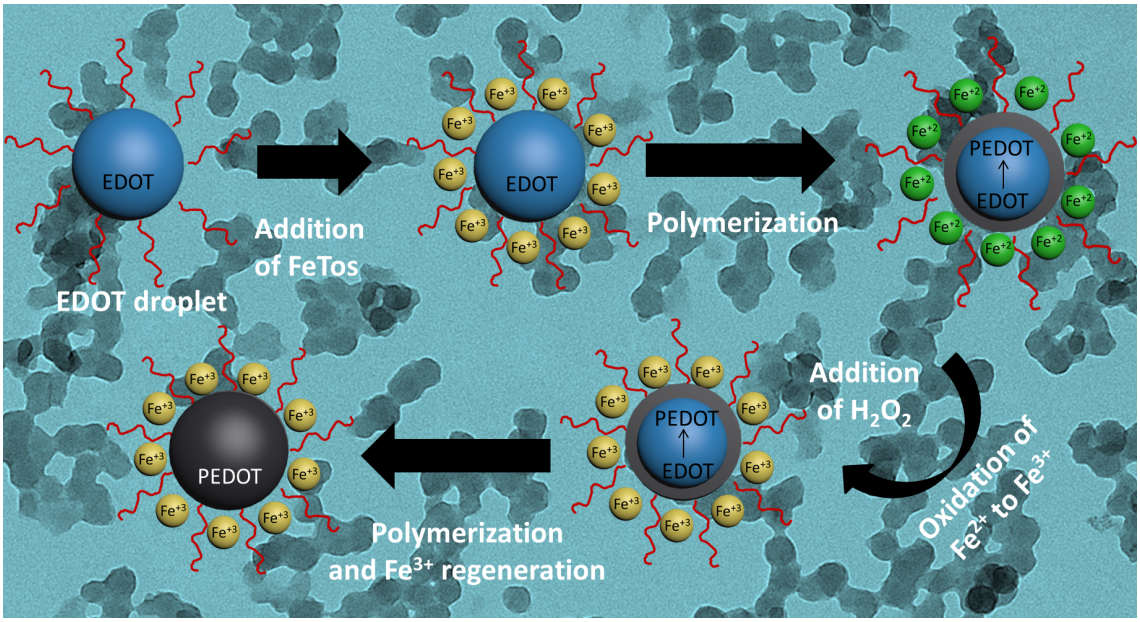
EDOT
EDOT droplet
Addition
of FeTos
EDOT
Polymerization
PEDOT
EDOT
Addition
of H_2O_2
Oxidation of
Fe^{2+} to Fe^{3+}
PEDOT
EDOT
Polymerization
and Fe^{3+} regeneration
PEDOT